Azadirachta indica (Neem) fruit latex based iron oxide magnetic nanoparticles (FeO-MNPs): Synthesis and green treatment of reactive yellow RY-176 dye

Ambreen Shahadat¹; environmentalistambreen@gmail.com:

Waqar Ahmed¹; <u>wahmeduok@gmail.com</u>:

Urooj Haroon^{2,*}; <u>uroojharoon@fuuast.edu.pk</u>:

Khalid Ahmed³; khalid.ahmed@Iccs.edu:

Highlights

- The synthesis of FeO-MNPs was carried out using a green approach without using harmful chemicals as reducing, capping or stabilizing agents.
- Latex of *Azadirachta indica* or unripe neem fruit was used in this green synthesis resulting in stable nanoscale particles between 2.5-24.5 nm in size by Atomic Force Microscopy (AFM).
- Synthesized nanoscale particles was examined for their effectiveness against Reactive Yellow RY-176 dye, revealing an impressive removal efficiency of 99 % at pH 4.
- The reusability efficiency was 78.52 % after three cycles.

Abstract

A considerable amount of wastewater is discharged by the textile industry primarily containing various pollutants, including dyes. The Reactive Yellow 176 dye is particularly notorious for its persistence and adverse effects on ecosystems. In response, the current work focuses on the preparation and application of iron oxide magnetic nanoparticles (FeO-MNPs), using unripe Azadirachta indica or Neem Fruit Latex (NFL) for the effective dye removal from aqueous media through the phenomena of adsorption. Iron oxide magnetic nanoparticles were synthesized using green co-precipitation method at mild temperature, employing Azadirachta indica fruit latex and ferric / ferrous chloride precursors. Various techniques of microscopy, spectroscopy, crystallographic and particle sizing were used to determine the synthesis of biogenic FeO-MNPs and for its characterization. Synthesized nanoparticles were in spherical shape with an average crystalline size of 16.5 nm, confirmed by X-ray Diffraction. The adjustability of the core size of particles, based on the latex concentration was confirmed by Atomic Force Microscopy whereas, Fourier Transform Infrared Spectroscopy demonstrated the presence of different functional groups that worked as reducing agents and contributed for stabilization of nanoparticles. These NFL based particles exhibited high adsorption capacity and rapid removal kinetics against reactive yellow 176 dye. Influence of dye concentration, pH and contact duration were thoroughly investigated, highlighting conditions that maximize removal capacity. For a dye concentration of 30 mg L⁻¹, 99.95 % removal efficiency was achieved at pH 4 with removal capacities of 29.89 mg g⁻¹ in 250 minutes and retained 78.52 % of their adsorption efficiency after three consecutive reuse cycles.

¹ Institute of Environmental Studies, University of Karachi, Karachi

² Department of Chemistry, Federal Urdu University Art, Science and Technology, Karachi

³ L. E. J. Nanotechnology Centre, H. E. J. Research Institute of Chemistry, ICCBS, University of Karachi

The adsorption process was best described by pseudo-second-order (PSO) kinetic model, indicating that chemical interactions played a significant role in dye removal. Overall, this study sheds light on the potential applications of biogenic iron oxide nanoparticles in industrial effluent treatment, providing an effective, efficient and ecofriendly approach to mitigate aquatic pollution.

Key Words: Reactive Yellow RY-176 dye; Iron oxide magnetic nanoparticles; Kinetic Models; Industrial Effluent Treatment and *Azadirachta indica* or Neem Fruit Latex (NFL).

1. INTRODUCTION

Contaminated water is the key ecological concern that is being faced all over the world induced by rapid industrialization and urbanization. This is largely due to the discharge of pharmaceutical active compounds and synthetic dyes in the industry's effluents (Sayed et al., 2024). Although the textile industry plays a vital role in driving global economic progress, it also carries the burden of contributing substantially to water pollution (Maruthai et al., 2025; Fernandes et al., 2019; Periyasamy, 2024). Among these, reactive yellow (RY) 176 dye stands out for its resilient nature and adverse environmental impact on the ecological system. It is a synthetic dye commonly used in textiles, inks and cosmetics. RY 176 is known for its vibrant yellow color and is frequently employed to achieve intense and long-lasting tones in products. It's a member of the azo dye family, a recalcitrant organic pollutant and has one or more nitrogen-nitrogen double bonds as its chromophoric groups, its complex chemical structure as mentioned in Figure (1). However, the widespread use of RY 176 dye has posed sever environmental concerns like persistence, toxicity, coloring of water bodies, effects on ecosystems and other regulatory concerns (Ahsan et al., 2022^a; Solomon et al., 2012). Consequently, the quest for advanced and efficient technologies for the removal of reactive yellow 176 has become imperative to mitigate the environmental consequences associated with textile dyeing processes (De Luca & Nagy, 2020).

In recent years, significant applications of nanotechnology have been demonstrated in various fields, including agriculture, biomedical, pharmaceutical, energy, multiple consumer goods, and others. It has also emerged as a promising avenue for tackling environmental challenges, offering innovative solutions to remediate water pollution (Selvanarayanan et al., 2024; Roy et al., 2022; Dye, 2017; Teoh et al., 2021). Nanomaterials have an advantage over other materials due to their extraordinary properties including porosity, thermal, optical, electrical, mechanical, magnetic ad particularly their size that range below 100 nm. Mostly Zinc, copper, silver, gold, cobalt, nickel and iron are used for the synthesis of nanoparticles (Karpagavinayagam & Vedhi, 2019; Ekwumemgbo et al., 2023; Dharshini et al., 2021; Niraimathee et al., 2016). Iron oxide nanoparticles have recently gained significance as versatile nanomaterials due to their wide array of application across multiple fields, such as specialized areas of medicine, cancer targeting, imaging, biosensing, therapeutic treatments, data storage, catalysis, energy and environment (Bibi et al., 2019; Ali et al., 2021; Patil et al., 2020; Zambri et al., 2019^a; Nadeem et al., 2022). Various types of iron oxide nanoparticles including γ-Fe₂O₃ (maghemite), Fe₃O₄ (magnetite) and α-Fe₂O₃ (hematite) widely used for multiple applications. These iron oxide nanoparticles can be synthesized through different chemical and physical techniques which include co-precipitation method, sol-gel technique, hydrothermal process, micro-emulsion, laser ablation and ball milling technique (Ting & Chin, 2020). Unfortunately, most of these techniques have drawbacks associated with them like high temperature requirements, extended time, usage of costly and noxious chemicals, low production and hazardous pollutants generation (Prasad et al., 2017; Madivoli et al., 2019). These drawbacks have led to greater emphasis on biological methods for synthesizing nanoparticles. In the context of sustainable development, exploration of nanoparticles

synthesis using plant extracts has earned significant attention as environmentally friendly substitute (Kanagasubbulakshmi & Kadirvelu, 2017^a; Prakash *et al.*, 2018).

Plant metabolites, including flavonoids, phenols, proteins, tannins, carbohydrates etc. not only facilitate nanoparticles reduction but also act as coating agents to stabilize and functionalize nanoparticles for versatile adsorption applications (Ahsan et al., 2022^b; Madubuonu et al., 2019). Azadirachta indica commonly known as neem is a fast-growing specie found across tropical regions and native to the Indian subcontinent. Ancient Indian literature comprehensively describes the medicinal properties of neem, detailing its uses in various forms such as fruits, seeds, oil, leaves, roots, and bark. It is highly valued for its phytochemicals constituents that offer huge benefits for human health and ecosystem (Chandramohan et al., 2016). The leaves extract of Azadirachta indica contain various phytochemicals including terpenoids and flavanones with major constituents such as nimbin, nimbidin, ninbidol, quercetin, salannin, azadirachtin etc. (Zambri et al., 2019b). These bioactive compounds have been effectively utilized in fabricating nanoparticles of various metals and metal oxides including calcium, silver, cobalt, cupric, iron, molybdate and zinc (Patil et al., 2022; Demirezen et al., 2019a). Few studies detailed the use of neem gum and latex for synthesizing silver nanoparticles and its potential applications as antimicrobial agent and catalyst (Velusamy et al., 2015; Al Aboody, 2019^a, Shahadat et al., 2024a). As the need for cost effective, sustainable and eco-friendly method for wastewater treatment is a global challenge, the current research focuses on the biofabrication of iron oxide magnetic nanoparticles (FeO-MNPs) using Azadirachta indica or neem fruit latex (NFL), a white milky juice that comes from unripe fruit. The co-precipitation technique was employed in this study as it is widely recognized as one of the simplest and most efficient pathway for synthesizing iron oxide nanoparticles with controllable size and shape (Bashir et al., 2020; Laurent et al., 2008). Based on the available literature, this study is the first to explore the use of Azadirachta indica or neem fruit latex for the biosynthesis of iron-oxide magnetic nanoparticles (FeO-MNPs) and its application for dye removal has not been reported yet.

Figure 1: Formula: C₂₉H₂₁ClN₈Na₄O₁₆S₅, Molecular Weight: 1025.26 g/mol, Molecular Structure: Azo Class, λ_{max} value: 420

The synthesized nanoparticles were used to evaluate their adsorption efficiency for dye (RY 176) removal to propose an effective wastewater treatment method. The results showed promising performance, confirming significant adsorption-based dye elimination capabilities. The behavior of the adsorption process and the interaction between the adsorbate (dye) with the adsorbent (iron nanoparticles) over time and other influencing factors were studied in detailed and the kinetic profile of the RY 176 dye by the synthesized nanoparticles (NPs) were established. This type of study is crucial for optimizing and designing efficient adsorption systems for the pollutants removal from industrial effluents before their discharged into the aquatic environment (Al Aboody, 2019^b).

2. METHODOLOGY

2.1 Materials

Unripe green fruit of *Azadirachta indica* or neem were picked in the morning from University of Karachi, Pakistan, Ferric (III) chloride hexahydrate (FeCl₃.6H₂O), Ferric (II) chloride tetrahydrate (FeCl₂.4H₂O) was used as Fe precursor, anionic reactive yellow dye (C₂₉H₂₁ClN₈Na₄O₁₆S₅), Deionized distilled water (DDW), sodium hydroxide (NaOH) and ethanol were purchased from Sigma Aldrich.

2.2 Preparation of Plant Material

Azadirachta indica unripe fruits were thoroughly rinsed with distilled water. Milky white latex as shown in **Figure (2A)** was collected drop by drop in a sterile glass container by gentle pressing. The solution was filtered twice with filter paper and stored at 4 °C for subsequent phytochemical analysis. Crude latex of 3 mL gently mixed with 100 mL DDW to prepare 3% latex solution. The solution was then used as plant material for further process.



Figure 2A: Milky white latex of unripe fruit of *Azadirachta indica*; 2B: Visible color changes from orange to brownish black with precipitates

2.3 Phytochemical Analysis of Neem Fruit Latex (NFL)

Phytochemical screening of *Azadirachta indica* or neem fruit latex was performed to explore the availability of secondary metabolites following the methods detailed by (Ahmed *et al.*, 2018; Vinay *et al.*, 2018; Kenneth *et al.*, 2017).

2.4 Biogenic Synthesis of Iron Oxide Magnetic Nanoparticles (Adsorbent)

The biogenic synthesis of magnetic iron oxide nanoparticles was carried out based on the methods reported by Danjuma *et al.*, 2022; Arsalani *et al.*, 2018) with certain modifications. Firstly, 13.5 g and 4.90 g of ferric (III) and (II) respectively, were dissolved separately in deionized distilled water at room temperature. Fe³⁺ solution was mixed with Fe²⁺ to achieve Fe³⁺/ Fe²⁺ molar ratio of 2:1. 50 mL of 3% neem fruit latex was added drop wise into 250ml of ferric chloride precursor and the mixture was agitated at 80 °C using a magnetic stirrer set at 500 rpm. The gradual addition of freshly prepared 2 M NaOH adjusted the pH to 10, leading to a color change from orange to brownish black with the precipitates formation. This transformation indicated the reduction of ferric chloride and the successful synthesis of iron oxide nanoparticles similar results reported by (Kanagasubbulakshmi & Kadirvelu, 2017^b; Mohandoss *et al.*, 2022). After resting at room temperature for 10 - 15 minutes, centrifuged at 4000 rpm for 15 minutes as part of the purification

step. The purification process was repeated three times, including washing with ethanol and then dried at 100 °C in a china dish resulting in black ferric oxide nanoparticles. The reactions involved are presented in equations 1 and 2.

$$FeCl_2.4H_2O + 2FeCl_3.6H_2O + 8NaOH \rightarrow Fe_3O_4(s) + 8NaCl + 20H_2O$$
 (1)

$$Fe^{2+} + 2Fe^{3+} + 8OH^{-1} \rightarrow Fe_3O_4 + 4H_2O$$
 (2)

2.5 Characterization of FeO-MNPs

Instruments used for characterization includes X-ray Diffractometer at 40 kV, 25 mA at 25 °C in the range from 2 theta = 5.0° to 80.0° , FTIR analysis by Bruker, Vector-22, Spectrophotometer in the range of 4000-400 cm⁻¹, Scanning Electron Microscopy 450 (dwell 10 μ s) Thermo Fisher Scientific armed with Energy Dispersive X-ray spectroscopy, Atomic Force Microscopy (AFM - 5500 Agilent Technologies) and UV-vis spectrophotometer Model-UV Thermo Scientific, (Evolution 300).

2.6 Adsorbate Reactive Yellow 176 Dye Adsorption Activity

A 30 mg L⁻¹ standard stock solution of RY176 was prepared in DDW. The initial pH of the dye solution was adjusted to 4, 7 and 9 and contact times ranging from 0 to 250 minutes were tested using a constant dose of FeO-MNPs (5 mg) adsorbent. The solution's pH was adjusted by using 0.1 M HCL and NaOH and change in color intensity was calculated using a UV-Vis Spectrophotometer at 420 nm. The RY176 dye removal efficiency was calculated using equation 3. Three replicates were performed for adsorption studies.

Adsorption Efficieny (%) =
$$\frac{\text{Ci} - \text{Ce}}{\text{Ci}} x \ 100 \%$$
 (3)

Where C_i and C_e represent the concentration of initial and equilibrium phase of RY 176 (mg L⁻¹) respectively. The amount of adsorbate (dye) adsorbed onto the adsorbent (iron nanoparticles) can be determined by using mass balance relationship as expressed by the equation 4.

Adsorption Capacity
$$(mg/g)$$
, $qe = \frac{Ci - Ce}{W} x V$ (4)

Where W denotes adsorbent weight in gram, and V corresponds to the solution volume in liters.

2.7 Adsorption Kinetic Model

The dye RY176 removal potential was assessed, and the adsorption isotherm was determined employing Langmuir, Freundlich and sips isothermal models. The equilibrium data were subsequently evaluated using kinetic models, specifically pseudo-first order (PFO) and pseudo-second order (PSO). The most common models used to study the kinetics of adsorption (Khatun *et al.* 2022). The correlation coefficient (R²) is considered as a measure of consistence between proposed models and experimental data for current study.

2.8 Reusability Analysis of FeO-MNPs

Reusability assays of synthesized NFL based FeO-MNPs were performed to assess their commercial applicability. Following the adsorption process, the nanoparticles rinsed with deionized water and dried at 70°C to achieve desorption. The recovered nanoparticles were then reused as adsorbent, and the procedure was repeated for three consecutive cycles by maintaining

other parameters i.e. dose of adsorbent, concentration of adsorbate, pH, and contact time throughout the experiments.

3. Result and Discussion

3.1 Screening of Phytochemical

Unripe neem fruit latex contains various bioactive compounds as listed in **Table 1**, which actively contribute to the formation of iron nanoparticles. Phenolic compounds, flavonoids, and tannins contain hydroxyl (-OH) and carboxyl (-COOH) groups, which can act as reducing agent by donating electrons to Fe³⁺ ions facilitating to their reduction into Fe²⁺ ions, a key step in Fe₃O₄ (magnetite) nanoparticle formation. These functional groups also act as capping agents preventing agglomeration and influencing their dispersion in aqueous solution. Similarly, aromatic rings present in flavonoids and other polyphenols can engage in π - π stacking interactions with iron oxide surface, enhancing nanoparticle stability.

Table 1: Screening of Phytochemicals in Azadirachta indica or Neem Fruit Latex (NFL)

Phytochemicals Components	Test	Interferences	
Alkaloids	Dragendroff's	+++	
Flavonoids	Lead acetate	+++	
Saponine (Frothing)	Frothing	++	
Phenolic Compounds	Ferric Chloride	+++	
Tannins	Braymer's	++	
Carbohydrates	Molish's	+	
Reducing Sugars	Benedict	++	
Glycosides (Cyanogenic)	Keller-Killani Test	++	

3.2 Visual observation of FeO-MNPs

The color of the solution (iron oxide nanoparticles with latex) changed from orange to brownish black with precipitate formation at the bottom as clearly observed in **Figure (2B)** indicating reduction in metal ions. According to Jayandran *et al.*, 2015 dark brown color clearly indicates the formation of well reduced and stabilized iron oxide nanoparticles. The optimal conditions for synthesizing iron oxide magnetic nanoparticles were found to be pH 10, temperature of 80°C and reaction time of 45-60 minutes. Furthermore, the resulting nanoparticles exhibit magnetic property in the aqueous solution attracted by external magnet field and deposited at the side of the magnetic rod as shown in **Figure (3A)** and **(3B)**. This phenomenon was observable only in the presence of applied magnetic fields suggestive of the formation of magnetic nanoparticles with a strong recommendation for recollect and reuse easily for the removal of dye. Notably, in the control experiment without neem latex, no color change and precipitate formation were observed, highlighting its essential role in the synthesis process.

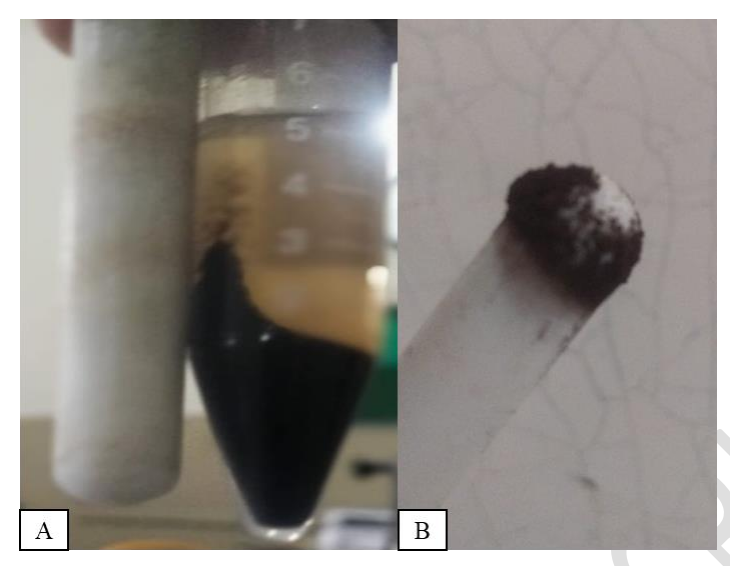


Figure 3A: Movement of FeO-MNPs due to external magnetic field; 3B: FeO-MNPs attracted at the side of magnetic rod

3.3. Assay through UV-Vis Spectrophotometry

UV visible spectroscopy is a critical tool for initial characterization of nanoparticles. Typically, iron oxide nanoparticles show absorption band around 280-420 nm as mentioned by Tyagi *et al.*, 2021; Pindiga *et al.*, 2023. UV-visible spectral analysis, as shown in **Figure (4)** displayed an intense absorbance at 324 nm with a band gap value of 3.27 eV ascribed to the excitation of surface plasmon resonance in the FeO-MNPs. High peak intensity is attributed to strong interaction between light and the oscillating surface electrons indicating photosensitivity of the synthesized particles as discussed by Pattanayak & Nayak, 2013).

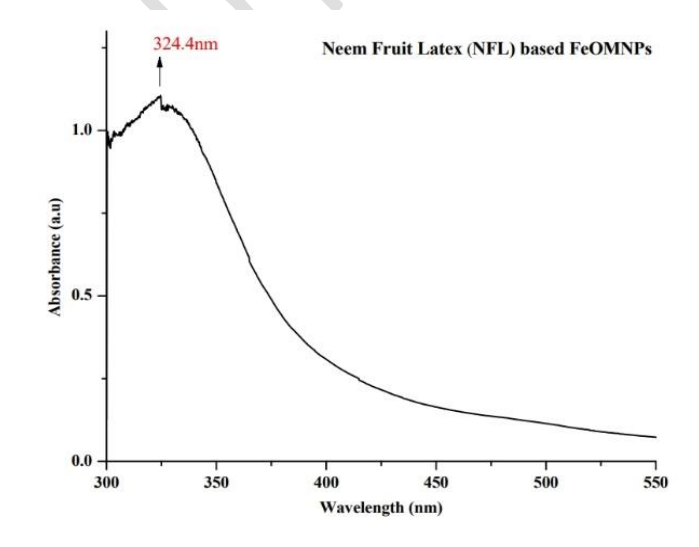


Figure 4: UV Spectrum of Azadirachta indica or neem fruit latex (NFL) based FeO-MNPs

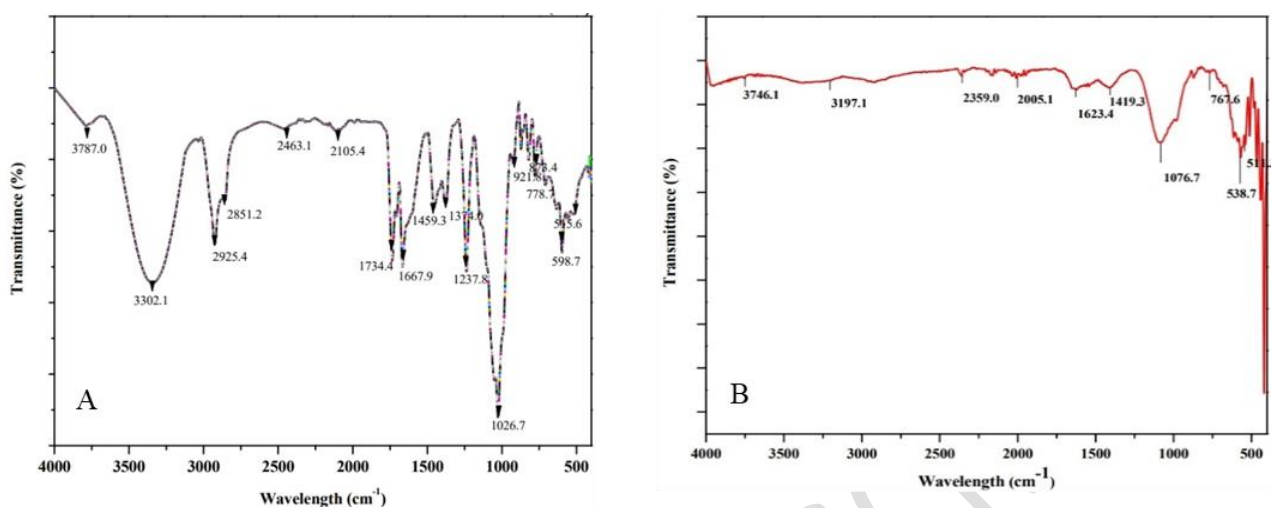


Figure 5A: FT-IR Spectrum of *Azadirachta indica* or neem fruit latex (NFL); 5B: FT-IR Spectrum of NFL based FeO-MNPs

3.4. Assay through FT-IR Spectroscopy

IR spectrum of the NFL demonstrated the presence of various functional groups through characteristic absorption bands, which were essential for the reduction, capping and stabilization as shown in Figure (5A) including hydroxyl group of phenols, -CH bond of alkyl, alkenyl and aryl groups, NH group of amines and amides, carbonyl (C=O) groups of aldehyde, ketones and amides, aryl C=C groups and C-O, C-N bonds of different organic molecules. FTIR spectra of FeO-MNPs observed varies peaks within the range of 400-4000 cm⁻¹ as depicts in Figure (5B) and confirmed the reducing role of neem fruit latex in the formation of FeO-MNPs. The peak at 3746.1 cm⁻¹ corresponds to the O – H stretching (free hydroxyl) due to moisture or phenolic groups whereas, broad O - H and N - H stretching denotes the hydrogen bonding from flavonoids or amines present in latex. $C \equiv C$ or CO_2 asymmetric stretching at 2359.0 cm⁻¹ indicates possible absorbed CO₂ or unsaturated groups and weak overtone relate to conjugated system at 2005.1 cm⁻¹. The strong peak at $1623.4 \text{ cm}^{-1} \text{ C} = \text{O}$ or C = C stretching (aromatic band) from flavonoids or tannins present in latex. O – H bending or COO⁻ symmetric stretch at 1419.3 cm⁻¹ indicative of carboxylic acids or esters whereas 1076.7 cm^{-1} is the C – O – C or C – O stretching confirms presence of polysaccharides or phenolic groups. Peak at 767.6 cm⁻¹ represents out-of-plane C – H bending related to aromatic compounds whereas, peaks at 538.7 cm⁻¹ and 511.3 cm⁻¹ are characteristic of metal-oxygen bonds (Fe – O) vibrations in the region of 550-500 cm⁻¹ confirm formation of iron oxide nanoparticles (Sudhakar et al., 2022). There was significant loss of IR absorption peaks in FeO-MNPs spectrum which suggests successful nanoparticle formation. The biomolecules act as reducing and stabilizing agents by donating electrons to reduce metal ions to their metallic states and often attach to the nanoparticle surface through coordination bond which causes their IR absorption peak to either weaken or disappear altogether.

3.5 Analysis through AFM Technique

AFM analysis showed that NFL based iron oxide NPS exhibited a size distribution between the ranges of 2.5 to 24.5nm with average particles of 22.5 nm as depicts in **Figure (6)**.

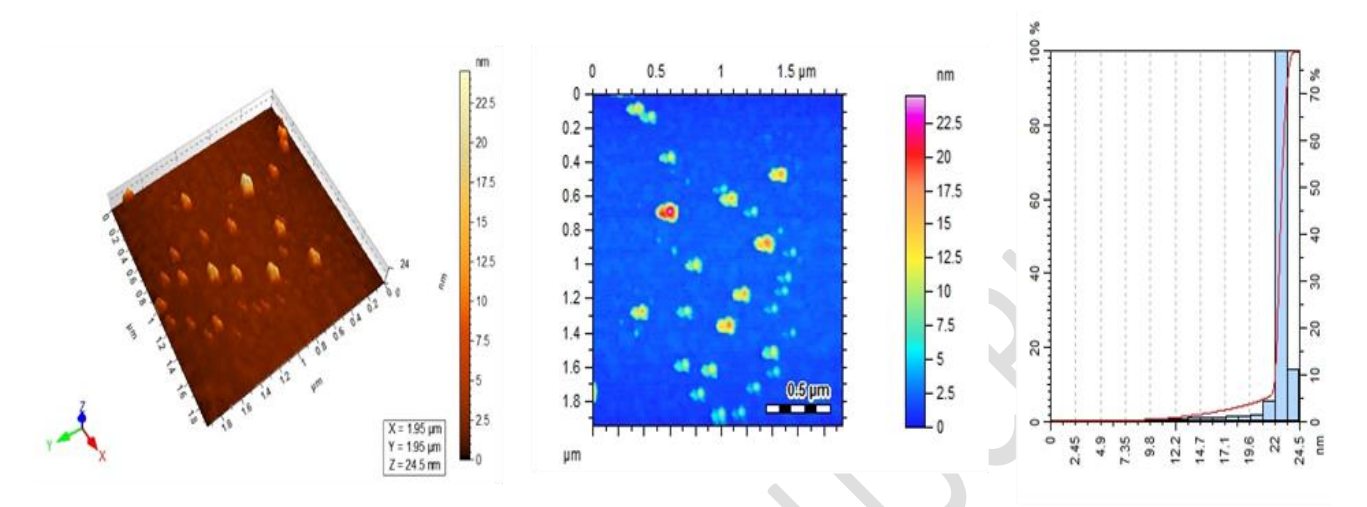


Figure 6: AFM images of Azadirachta indica or neem fruit latex (NFL) based FeO-MNPs

3.6 Analysis through SEM and EDX

analysis revealed that FeO-MNPS exhibited various shapes, predominantly irregular, with spherical and granular structure and cubic phase structure (close-packed structure), ranging in size from 20.59 to 84.58 nm with several agglomerates as shown in Figure (7) due to magnetic attraction generated by individual FeO-MNPs. Different plant based iron oxide nanoparticles synthesis reported variations in size using SEM techniques like Azadirachta indica (neem) leaf extract has been utilized for one pot synthesis of iron oxide nanoparticles which exhibited irregular morphology and average size of 9-12 nm (Zambri et al., 2019°). Black carrot (Daucus carota subsp. sativus) vegetable extracts were also employed which produced nanoscale particles that exhibited quasi-spherical shape, with varying sizes from 80-103 nm (Uncu Kirtiş et al., 2025). Phyllanthus niruri extract was utilized in another green approach synthesis spherical iron oxide nanoparticles with an average size of approximately 12.34 nm (VG , 2018). Similarly, Hibiscus rosa-sinensis flower extract was used in a microwave assisted synthesis method. The nanoparticles were in the range of 20-40 nm and mostly spherical in shape (Buarki et al., 2022). In our study we have introduced neem Azadirachta indica or neem fruit latex a novel green approach used for the iron oxide nanoparticles synthesis. EDX analysis was performed for further assessing the stoichiometry and element composition of the iron oxide nanoparticles as mentioned in Table 2. The appearance of clear peaks shown in Figure (8) at 6.4 and 7.2 keV associated with obligatory energies of iron (Fe) whereas, oxygen (O) peak appears strongly exhibits highest intensity at around 0.5 keV reinforcing the possibility of iron

oxide structure in which Fe atoms are chemically bonded with O (Dhar et al., 2021 & Sirdeshpande et al., 2018).

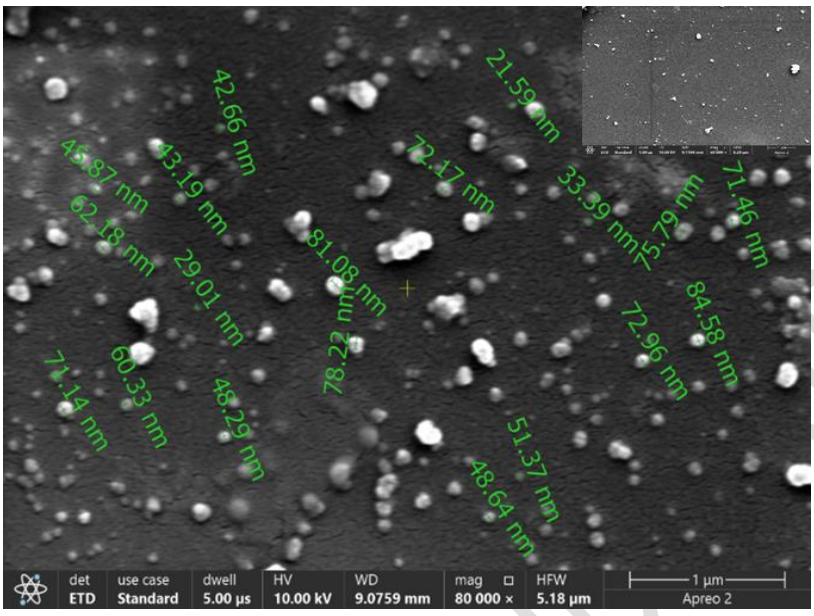


Figure 7: SEM results of Azadirachta indica or neem fruit latex (NFL) based FeO-MNPs

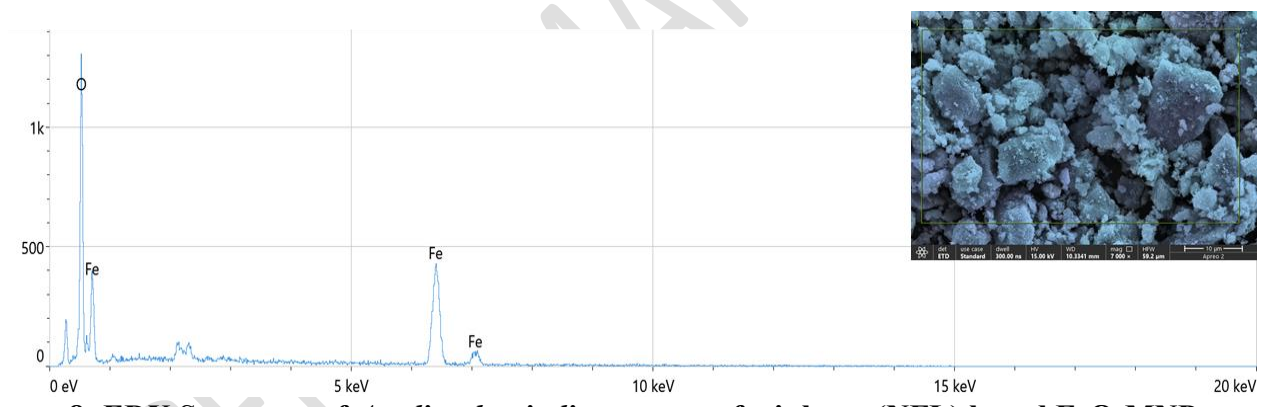


Figure 8: EDX Spectrum of Azadirachta indica or neem fruit latex (NFL) based FeO-MNPs

Table 2: Elemental Composition of NFL based FeO-MNPs

Elements Atomic (%)		Error	Weight (%)	Error	
0	53	0.9	25.2	0.4	
Fe	46	1.0	75.0	1.6	

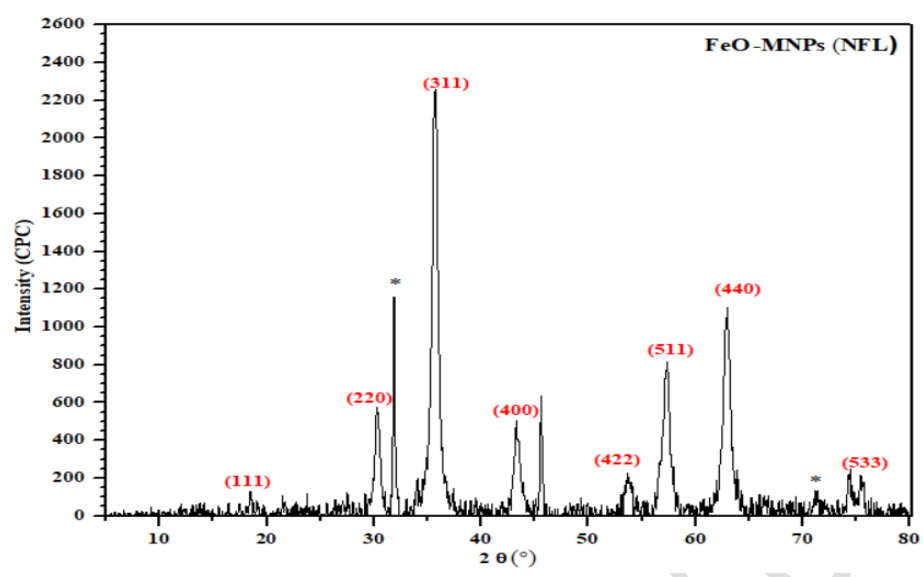


Figure 9: XRD Spectrum of *Azadirachta indica* or neem fruit latex (NFL) based FeO – MNPs

3.7. Analysis by XRD

Figure (9) displays diffraction peaks at 18.6° 30.4° , 35.7° , 43.3° , 53.6° , 57.3° and 63.0° corresponded to the (111), (220), (311), (400), (422), (511), and (440) planes respectively confirming the single-phase crystalline nature of the iron oxide nanoparticles matching exactly to the JCPDS No .19-629. Usha *et al.*, 2022 & Majid *et al.*, 2021 obtained similar results in which distinct peak of Fe₃O₄ was observed at 30.47 (20) and intense peak at 20 = 35.96. The XRD spectrum displayed the sharp and narrow diffraction peaks suggesting that the synthesized FeO-MNPs were both pure and highly crystalline. They exhibited a distinct rhombohedral crystalline nature, consistent with the findings reported by (Yazdani & Seddigh, 2016; Stan *et al.*, 2017 & Chinyerenwa *et al.*, 2018). The XRD pattern confirmed the crystalline size of synthesized FeO-MNPs and average particle size calculated by employing Debye-Scherrer formula was 16.5 nm.

3.8 Analysis by DLS

Dynamic Light scattering (DLS), measures the hydrodynamic size of nanoparticles which is generally larger as compared to microscopic size which represents only the actual core of nanoparticles. This increase in size is mainly due to particle aggregation in aqueous solution, which is a typical phenomenon for iron nanoparticles due to high surface energy and magnetic interactions which impacts their colloidal stability in water-based applications. Furthermore, the presence of biological material used as capping agents can also contribute to an increase in the hydrodynamic size. Polydispersibility index (PDI) was found to be 2163 ± 0.455 d-nm with an intercept value of 0.930 whereas zeta potential was found -12.6 mv as shown in **Figure (10)**, which indicated moderate repulsive forces between the particles and reasonable stability in the colloidal

state. Even though stability is typically greater when zeta potential is higher than +20 mV or less than -20 mV, however the measured value suggests a balance that prevents significant aggregation (Nwamezie & Igwe, 2018).

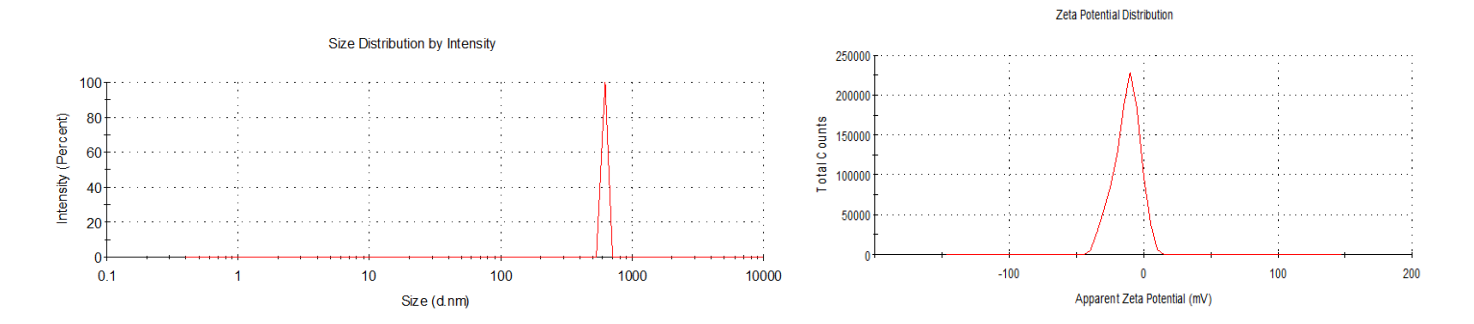


Figure 10: DLS Spectrum of *Azadirachta indica* or neem fruit latex (NFL) based FeO-MNPs

3.9 Adsorption Kinetic and Isotherms Modeling

The results showed that synthesized magnetic nanoparticles demonstrated favorable properties that positioned them to be used for treating wastewater contaminated with synthetic dyes. Following this, FeO-MNPs were further evaluated for their adsorption potential in removing reactive yellow 176 dye through adsorption kinetics and isotherm modeling. Reactive yellow 176 is an anionic dye containing negatively charged sulfonate groups which could interact with the surface hydroxyl groups of iron oxide nanoparticles particularly at lower pH promoting strong electrostatic attractions. The nanoparticles surface hydroxyl groups could also form hydrogen bonding with functional groups present in the dye, such as amide (-NH₂) and hydroxyl (-OH) groups. Also, the aromatic rings and conjugated azo (-N=N-) system in Reactive Yellow 176 could facilitate π - π stacking interactions with the iron oxide nanoparticle surface, further stabilizing dye adsorption.

Table 3: Effects of pH on removal efficiency & capacity of RY-176 dye with FeO-MNPs

pН	pH C ₀ (mg L ⁻¹)		Removal Capacity	
		%	$(mg g^{-1})$	
Acidic (4)	30	99.95	29.89	
Neutral (7)	30	95.18	28.34	
Basic (9)	30	19.27	5.84	

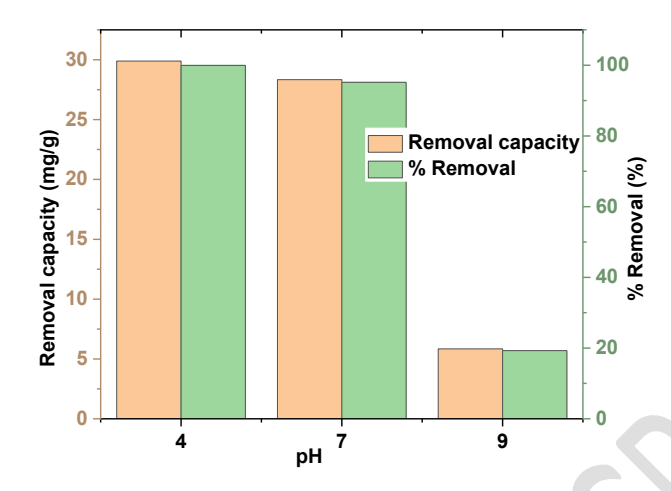


Figure 11: Effects of pH on removal efficiency & capacity of RY-176 dye with FeO-MNPs
3.10 Impact of Experimental Variables on the Adsorption Process
pH of Solution

The effect of pH on the removal efficiency of iron oxide nanoparticles for removal of RY-176 dye showed that acidic conditions enhanced both parameters, while alkaline conditions significantly hindered them. At an initial concentration of 30 mgL⁻¹, the percent removal was 99.95%, 95.18%, and 19.27% at pH 4, 7, and 9, respectively, with corresponding removal capacities of 29.89, 28.34, and 5.84 mg g⁻¹ as shown in **Table 3** and **Figure (11)**. The high removal capacity at pH 4 suggests favorable electrostatic interactions between the dye molecules at the nanoparticle surface. In contrast, the decrease at neutral pH and further decline at pH 9 indicated that an increasingly negative surface charge in alkaline conditions likely caused repulsion with the dye, reducing adsorption effectiveness. This trend highlights the importance of acidic pH for optimizing iron oxide nanoparticles in dye removal applications.

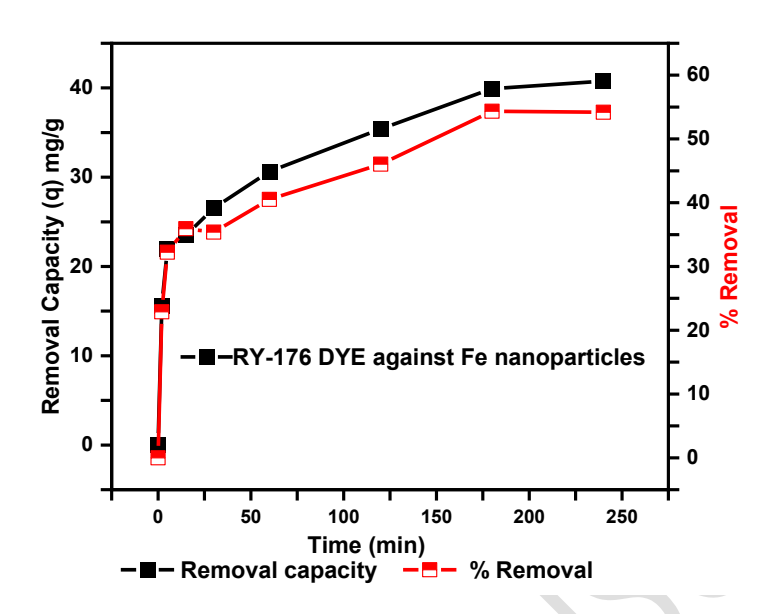


Figure 12: Effects of time on removal efficiency & capacity of RY-176 dye with FeO-MNPs

Contact duration

The contact time between iron oxide nanoparticles and the dye is a critical factor in the dye removal process, impacting both the % removal and removal capacity. This was demonstrated in experiments using 30 mgL⁻¹ dye solution with 5 mg iron oxide nanoparticles at 298 K in acidic conditions across varying durations as shown in **Figure (12)**. In the initial 25 minutes, rapid removal was observed, with 35% of dye removed and a removal capacity of 25 mg/g, attributed to the abundance of active sites on the nanoparticles surface. Over time, the % removal and removal capacity gradually increased, achieving approximately 60% removal and 40 mg g⁻¹ removal capacity by 250 minutes. This slower removal rate in later stages is likely due to the reduction in available active sites and saturation effects, suggesting an optimal contact time of 250 minutes for maximum removal efficiency. Under optimal conditions at pH 4, the dye removal reached 99.95% with removal capacity of 29.89 mg/g, while increasing pH to 7 and 9 reduced the removal efficiency to 95.18% and 19.27%, with corresponding removal capacities of 28.34 mg g⁻¹ and 5.84 mg g⁻¹, respectively.

Table 4: Kinetic parameters of Pseudo-first-order (PFO) and Pseudo-second-order (PSO) models for the RY-176 dye removal

Material	Conc.	Pseudo-first-order kinetic		Pseudo-second-order kinetic			
	mg L ⁻¹	model		model			
		q _e	k_1	\mathbb{R}^2	qe	k_2	R^2
		mmol g ⁻¹	min ⁻¹		mmolg ⁻¹	mmol g ⁻¹ min ⁻	
FeO-MNPs	30	33.340	0.212	0.82	36.499	0.006	0.90

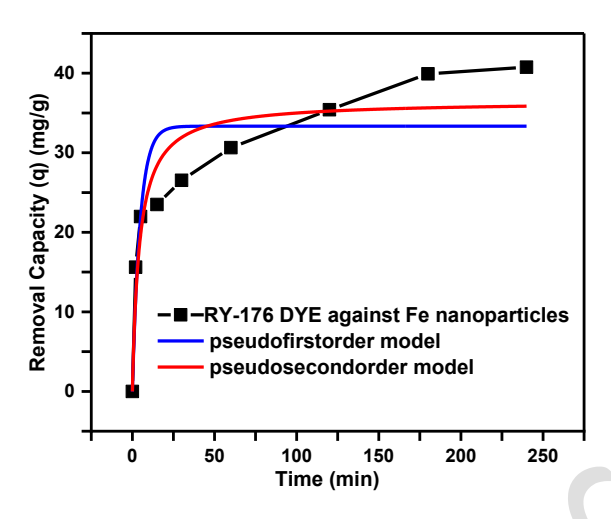


Figure 13: Kinetic isotherms for the removal of RY-176 dye and experimental data with adjustment to PFO and PSO Models

Adsorption kinetics

Kinetic studies offer valuable insights into the removal mechanism by modeling removal rates and fitting experimental data into kinetic models. In this work, the removal kinetics of a 30 mg L⁻¹ dye solution with iron oxide nanoparticles at 298 K were analyzed using pseudo-first-order (PFO) and pseudo-second-order (PSO) models (Ahmed *et al.*, 2018; Agbovi & Wilson., 2021; Ahmed *et al.*, 2016). The equations for the kinetic models are provided below in equation 5 & 6.

(PFO)
$$q_t = q_e(1 - e^{-k_1 t})$$
 (5)

(PSO)
$$q_t = \frac{q_e^2 k_2 t}{1 + q_e k_2 t}$$
 (6)

Where, q_e represents the removal capacity of the adsorbent (mg g^{-1}) at equilibrium, while qt represents the capacity of adsorption at 't' time interval. The parameters k_1 and k_2 represent to the PFO and PSO rate constant, respectively. Plotting non-linear graph of qt against t provides the values of the rate constant (k) and q_e as shown in **Table 4** and **Figure (13)**.

For the PFO model, the removal capacity at equilibrium (q_e) was found to be 33.34 mmol g⁻¹, with a rate constant K of 0.212 min⁻¹ and a correlation coefficient R² of 0.82, suggesting a moderate fit. Conversely, the PSO model provided a slightly higher (q_e) of 36.49 mmol g⁻¹ and a lower rate constant K of 0.006 mmol g⁻¹ min⁻¹, with an improved R² of 0.90. The higher correlation coefficient in the PSO model, suggests a more accurate depiction of the removal process. The better fit of the PSO model implies that the degradation rate is controlled by chemisorption, involving valence forces through sharing or exchange of electrons between dye molecules and active sites on the nanoparticles. This interaction leads to a slower, yet more stable, degradation process as equilibrium is reached. Therefore, the PSO model highlights the strong chemical affinity involved in the adsorption process and provides a more reliable framework for predicting dye removal efficiency over extended contact times in aqueous system.

Table 5: Removal of RY-176 dye using different adsorption models

Adsorption Models	FeO-MNPs			
Langmuir				
Q _{max} (mmol g ⁻¹)	123.68±4.90			
$K_L (dm^3mg^{-1})$	0.027			
R^2	0.986			
Freundlich				
n	4.203±0.64			
$K_{\rm f}$ [mmol g ⁻¹ (mg dm ⁻³) ^{-1/n}]	28.653±5.20			
\mathbb{R}^2	0.969			
Sips				
Q _{max} (mg g ⁻¹)	128.793±17.15			
K _s [(mg dm ⁻³) ^{-1/n}]	0.0385			
n_s	1.127±0.36			
\mathbb{R}^2	0.987			

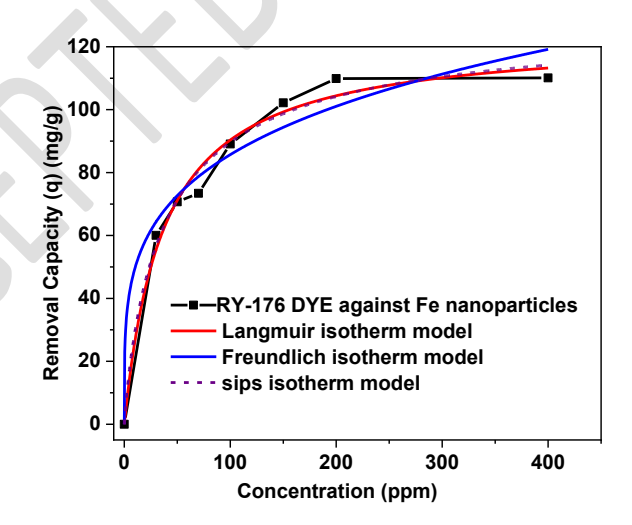


Figure 14: Adsorption Isotherms with adjustment to Langmuir, Freundlich and Sips Models

Adsorption Isotherm

The removal equilibrium investigates the distribution of dye molecules between iron oxide nanoparticles and the solution when the equilibrium is attained. This analysis considers the concentration of the dye to understand the extent to which it partitions between the two phases. In this study, the Langmuir, Freundlich, and Sips isotherms, well-known models, were explored across a range of dye concentrations. The objective was to elucidate the maximum removal capacity (q_{max}) and the removal mechanism of the nanoparticle. The Langmuir adsorption isotherm, which assumes monolayer adsorption on a homogeneous surface, was employed for this purpose as mentioned in equation 7 (Sayed et al., 2024; Ali et al., 2024).

$$q_e = \frac{q_m K_L C_e}{1 + K_L C_e} \tag{7}$$

Here, q_m (mg g^{-1}) denotes the highest adsorption capacity, indicating the maximum quantity of dye that can be adsorbed per unit mass of adsorbent. K_L (dm³ mg⁻¹), the Langmuir constant, reflects the affinity of the nanoparticles for the dye. The Freundlich isotherm, on the other hand, describes multilayer adsorption occurring on a heterogeneous surface, as mentioned below in equation 8.

$$q_e = K_F C^{\frac{1}{n}} \tag{8}$$

In this equation, qe denotes the removal equilibrium capacity (mg g⁻¹), while Ce represents the equilibrium concentration after removal. K_F is the Freundlich constant, The Sips adsorption model, which is frequently employed in adsorption studies, combines aspects of both the Langmuir and Freundlich models. It can be mathematically expressed as mentioned in equation 9.

$$q_e = \frac{Q_{max} K_s C_{eq}^{\frac{1}{ns}}}{1 + K_s C_{eq}^{\frac{1}{ns}}}$$

$$(9)$$

Where qe denotes equilibrium removal capacity, measured in mg g⁻¹, while Ceq denotes the concentration of the dye at equilibrium in the solution, expressed in mg L⁻¹. Ks stands for the Sips constant and is measured in dm³ mg⁻¹.

The adsorption isotherms for dye removal by iron oxide nanoparticles indicate that each of the Langmuir, Freundlich, and Sips models provided useful insights into the removal process. In the Langmuir model, with a high $Q_{max} = 123.68$ mmol g^{-1} , $K_L = 0.27$, and $R^2 = 0.986$, the data suggest a strong affinity for dye molecules forming a monolayer on homogeneous surface sites, reflecting efficient initial removal adsorption that may support degradation as shown in **Table 5** and **Figure (14)**. The Freundlich model, with n = 4.20, $K_f = 28.65$, and $R^2 = 0.969$ further confirmed this process with a favorable adsorption intensity n > 1, indicating multilayer adsorption on heterogeneous surfaces, which might enhance interaction sites for degradation reactions. The Sips model, which is Langmuir and Freundlich models hybrid, yielded a slightly higher Q_{max} of 128.79 mg g^{-1} , with K = 0.038, n = 1.127, and $R^2 = 0.987$, showing the system's adaptability to both low and high dye concentrations. The strong correlation values (close to 1) in each model suggest high reliability in describing the dye removal mechanism, with the Sips model slightly outperforming in fitting data. The findings suggest that the dye removal by iron oxide nanoparticles occurred

through a two-step process: an initial adsorption phase followed by degradation mediated via surface interactions.

3.12 Multiple Reusability of FeO-MNPs

The reusability of adsorbent FeO-MNPs is important to decrease the production cost. The percentage of removal decrease from cycle 1 to 3 with following the conditions like pH 4, concentration 30 mg L⁻¹, dosage of adsorbate 5 mg and time 150 mins. The removal of RY176 dye achieved up to 95.45% in 1st cycle after 3rd run removal efficiency decreased to 78.52% as mentioned in **Figure (15)** due to blockage of the active sites of adsorbate. During recovery phase, it is found very easy to recover the FeO-MNPs with minimal loss due to its magnetic nature during recovery phase.

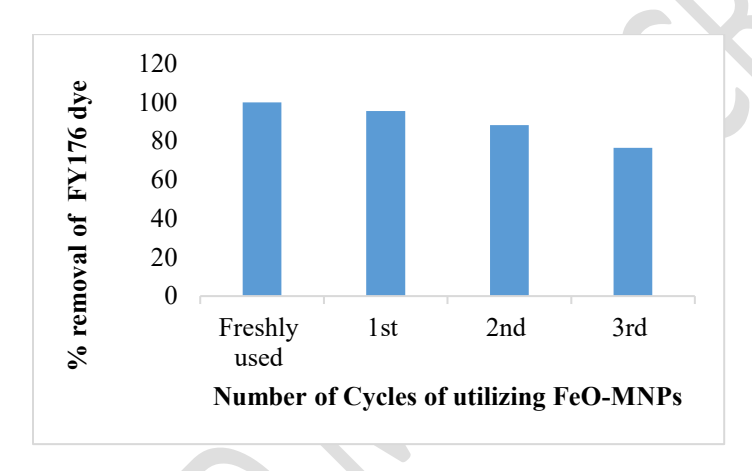


Figure 15: Multiple reusability of FeO-MNPs for RY 176 dye removal

4. Conclusion

This latex-based biosynthetic method for FeO-MNPs offers a sustainable, cost-effective route for dye remediation, with promising implications for industrial wastewater treatment. The nanoparticles demonstrated high reactivity in effectively removing reactive yellow 176 dye. The careful synthesis and application of these nanoparticles for scouring pollutants from industrial effluents underscore their promise as an eco-friendly solution for wastewater treatment. Azadirachta indica (Neem) fruit latex substantiates the presence of variety of chemicals including phenols, alkaloids etc. mediates in reduction process and act as capping agent in the synthesis of FeO-MNPs. Furthermore, this study showed that Pseudo-second order (PSO) is the best fitted adsorption kinetics indicating chemisorption controlled process whereas the Sips model was provided the best fitting adsorption isotherm as compare to Langmuir and Freundlich. Overall, FeO-MNPs found to be alternative option for wastewater treatment

References

- Agbovi, H. K. and Wilson, L. D. (2021). Adsorption processes in biopolymer systems: fundamentals to practical applications. In Natural polymers-based green adsorbents for water treatment (pp. 1-51). *Elsevier*.
- Ahmed, K., Khan, A. J., Pires, C. T., Yamin, M., Rehman, F., Rahim, A. and Airoldi, C. (2018). Fabrication of layered Al-silicate magadiites for the removal of reactive dyes from textile effluents. *Desalination and Water Treatment*, **104**, 159-168.
- Ahmed, K., Rehman, F., Pires, C. T., Rahim, A., Santos, A. L. and Airoldi, C. (2016). Aluminum doped mesoporous silica SBA-15 for the removal of remazol yellow dye from water. *Microporous and Mesoporous Materials*, **236**, 167-175.
- Ahmed, S. H., Hameed, R. H., Thamir, H., Mohammed, H., Al-Roomi, R., Hussain, I. and Al-Karkhi, T. (2018). Production of iron nanoparticle by using *Aloe vera* gel and studying its effect on *Lepidium sativum* seed germination. *International Journal of Bioscience*, **13**, 248-55.
- Ahsan, H., Shahid, M., Imran, M., Mahmood, F., Siddique, M. H., Ali, H. M. and Shahzad, T. (2022). Photocatalysis and adsorption kinetics of azo dyes by nanoparticles of nickel oxide and copper oxide and their nanocomposite in an aqueous medium. *Peer J*, **10**, e14358.
- Al Aboody, M. S. (2019). Silver/silver chloride (Ag/AgCl) nanoparticles synthesized from *Azadirachta indica* latex and its antibiofilm activity against fluconazole resistant *Candida tropicalis*. *Artificial Cells*, *Nanomedicine*, *and Biotechnology*, **47**(1), 2107-2113.
- Ali, A., Shah, T., Ullah, R., Zhou, P., Guo, M., Ovais, M., Tan, Z., & Rui, Y. (2021). Review on recent progress in magnetic nanoparticles: Synthesis, characterization, and diverse applications. *Frontiers in Chemistry*, **9**, 629054.
- Ali, E. A., Elsaid, K., Hughes, D. J., Nasef, M. M., Syed, J. A., Ali, M. and Ghouri, Z. K. (2024). N-doped and Se incorporated reduced graphene oxide nanocomposite as a new adsorbent for efficient Ni (II) ion removal from aqueous sample. *Emergent Materials*, 7(3), 1031-1042.
- Arsalani, S., Guidelli, E. J., Araujo, J. F., Bruno, A. C. and Baffa, O. (2018). Green synthesis and surface modification of iron oxide nanoparticles with enhanced magnetization using natural rubber latex. *ACS Sustainable Chemistry & Engineering*, **6**(11), 13756-13765.
- Bashir, M., Ali, S. and Farrukh, M. A. (2020). Green synthesis of Fe₂O₃ nanoparticles from orange peel extract and a study of its antibacterial activity. *Journal of the Korean Physical Society*, **76**, 848-854.
- Bibi, I., Nazar, N., Ata, S., Sultan, M., Ali, A., Abbas, A. and Iqbal, M. (2019). Green synthesis of iron oxide nanoparticles using pomegranate seeds extract and photocatalytic activity evaluation for the degradation of textile dye. *Journal of Materials Research and Technology*, **8**(6), 6115-6124.
- Buarki, F., AbuHassan, H., Al Hannan, F., & Henari, F. (2022). Green synthesis of iron oxide nanoparticles using *Hibiscus rosa sinensis* flowers and their antibacterial activity. *Journal of Nanotechnology*, **2022**(1), 5474645.
- Chandramohan, B., Murugan, K., Panneerselvam, C., Madhiyazhagan, P., Chandirasekar, R., Dinesh, D. and Benelli, G. (2016). Characterization and mosquitocidal potential of neem cake-synthesized silver nanoparticles: genotoxicity and impact on predation efficiency of mosquito natural enemies. *Parasitology Research*, **115**, 1015-1025.

- Chinyerenwa, A. C., Munna, M. K. H., Rahman, S., Mia, M. R., Yousuf, M. A. and Hasan, J. (2018). Ecofriendly sweet scented *Osmanthus* leaf extract mediated synthesis of silver nanoparticles (SNPs). *International Journal of Textile Science*, 7, 35-42.
- Danjuma, M. S., Adamu, A., Kumar, S. A. and Umar Kura, N. (2022). Eco-friendly synthesis and characterization of iron nanoparticles using crude extract from *Eucalyptus globulus* leaves as reducing and capping agents. *Nanochemistry Research*, 7(2), 135-142.
- De Luca, P. & B. Nagy, J. (2020). Treatment of water contaminated with reactive black-5 dye by carbon nanotubes. *Materials*, **13**(23), 5508.
- Demirezen, D. A., Yıldız, Y. Ş., Yılmaz, Ş., & Yılmaz, D. D. (2019). Green synthesis and characterization of iron oxide nanoparticles using Ficus carica (common fig) dried fruit extract. *Journal of bioscience and bioengineering*, **127**(2), 241-245.
- Dhar, P. K., Saha, P., Hasan, M. K., Amin, M. K. and Haque, M. R. (2021). Green synthesis of magnetite nanoparticles using *Lathyrus sativus* peel extract and evaluation of their catalytic activity. *Cleaner Engineering and Technology*, **3**, 100117.
- Dharshini, R. S., Poonkothai, M., Srinivasan, P., Mythili, R., Syed, A., Elgorban, A. M. and Kim, W. (2021). Nano-decolorization of methylene blue by *Phyllanthus reticulatus* iron nanoparticles: an eco-friendly synthesis and its antimicrobial, phytotoxicity study. *Applied Nanoscience*, 1-11.
- Dye, I. A. O. (2017). Green synthesis of superparamagnetic iron oxide nanoparticle from Ficus carica fruit extract, characterization studies and its application on dye degradation studies. *Asian Journal of Pharmaceutical and Clinical Research*, **10**(3), 125-128.
- Ekwumemgbo, P. A., Shallangwa, G. A. and Okon, I. E. (2023). Green synthesis and characterization of iron oxide nanoparticles using *Prosopis africana* leaf extract. *Communication in Physical Sciences*, 9(2).
- Fernandes, R. J., Magalhães, C. A., Amorim, C. O., Amaral, V. S., Almeida, B. G., Castanheira, E. M. and Coutinho, P. J. (2019). Magnetic nanoparticles of zinc/calcium ferrite decorated with silver for photodegradation of dyes. *Materials*, **12**(21), 3582.
- Jayandran, M., Haneefa, M. M. and Balasubramanian, V. (2015). Green synthesis of copper nanoparticles using natural reducer and stabilizer and an evaluation of antimicrobial activity. *Journal of Chemical and Pharmaceutical Research*, 7(2), 251-259.
- Kamaraj, M., Kidane, T., Muluken, K. U. and Aravind, J. (2019). Biofabrication of iron oxide nanoparticles as a potential photocatalyst for dye degradation with antimicrobial activity. *International Journal of Environmental Science and Technology*, **16**, 8305-8314.
- Kanagasubbulakshmi, S. and Kadirvelu, K. J. D. L. S. J. (2017). Green synthesis of iron oxide nanoparticles using *Lagenaria siceraria* and evaluation of its antimicrobial activity. *Defence Life Science Journal*, **2**(4), 422-427.
- Karpagavinayagam, P. and Vedhi, C. (2019). Green synthesis of iron oxide nanoparticles using Avicennia marina flower extract. *Vacuum*, **160**, 286-292.
- Kenneth, E., Paul, T., Istifanus, N., Uba, U., Rejoice, A., Victor, O. and Mohammed, S. (2017). Phytochemical analysis and antibacterial activity of *Psidium guajava L*. leaf extracts. *GSC Biological and Pharmaceutical Sciences*, **1**(2), 13-19.

- Khatun, R., Mamun, M. S. A., Islam, S., Khatun, N., Hakim, M., Hossain, M. S. and Barai, H. R. (2022). Phytochemical-assisted Synthesis of Fe3O4 Nanoparticles and Evaluation of Their Catalytic Activity. *Micromachines*, **13**(12), 2077.
- Laurent, S., Forge, D., Port, M., Roch, A., Robic, C., Vander Elst, L. and Muller, R. N. (2008). Magnetic iron oxide nanoparticles: synthesis, stabilization, vectorization, physicochemical characterizations, and biological applications. *Chemical Reviews*, **108**(6), 2064-2110.
- Madivoli, E. S., Kareru, P. G., Gachanja, A. N., Mugo, S. M. and Makhanu, D. S. (2019). Phytofabrication of iron nanoparticles and their catalytic activity. *SN Applied Sciences*, **1**, 1-8.
- Madubuonu, N., Aisida, S. O., Ali, A., Ahmad, I., Zhao, T. K., Botha, S. and Ezema, F. I. (2019). Biosynthesis of iron oxide nanoparticles via a composite of *Psidium guavaja-Moringa oleifera* and their antibacterial and photocatalytic study. *Journal of Photochemistry and Photobiology B: Biology*, **199**, 111601
- Majid, A., Naz, F., Jamro, H. A., Ansari, B., Abbasi, S., Lal, S. and Ujjan, S. A. (2021). Facile green synthesis of iron oxide nanoparticles using *Phoenix dactylifera L*. seed extract and their antibacterial applications. *Journal of Pharmaceutical Research International*, **33**, 21-29.
- Maruthai, S., Rajendran, S., Selvanarayanan, R., & Gowri, S. (2025). Wastewater recycling integration with IoT sensor vision for real-time monitoring and transforming polluted ponds into clean ponds using HG-RNN. *Global Nest Journal*, 27(4).
- Mohandoss, N., Renganathan, S., Subramaniyan, V., Nagarajan, P., Elavarasan, V., Subramaniyan, P. and Vijayakumar, S. (2022). Investigation of biofabricated iron oxide nanoparticles for antimicrobial and anticancer efficiencies. *Applied Sciences*, **12**(24), 12986.
- Nadeem, F., Fozia, F., Aslam, M., Ahmad, I., Ahmad, S., Ullah, R. and Abdel-Daim, M. M. (2022). Characterization, antiplasmodial and cytotoxic activities of green synthesized Iron Oxide nanoparticles using *Nephrolepis exaltata* aqueous extract. *Molecules*, **27**(15), 4931.
- Niraimathee, V. A., Subha, V., Ravindran, R. E. and Renganathan, S. (2016). Green synthesis of iron oxide nanoparticles from *Mimosa pudica* root extract. *International Journal of Environment and Sustainable Development*, **15**(3), 227-240.
- Nwamezie, F. and Igwe O. U. (2018). Green synthesis of iron nanoparticles using flower extract of *Piliostigma thonningii* and their antibacterial activity evaluation. *Chem. Int*, **4**(1), 60.
- Patil, S. P., Chaudhari, R. Y. and Nemade, M. S. (2022). Azadirachta indica leaves mediated green synthesis of metal oxide nanoparticles: A review. *Talanta Open*, **5**, 100083.
- Patil, Y. Y., Sutar, V. B. and Tiwari, A. P. (2020). Green synthesis of magnetic iron nanoparticles using medicinal plant *Tridax procumbens* leaf extracts and its application as an antimicrobial agent against E. coli. *International Journal of Applied Pharmaceutics*, **12**, 34-39.
- Pattanayak, M. and Nayak, P. L. (2013). Ecofriendly green synthesis of iron nanoparticles from various plants and spices extract. *International Journal of Plant, Animal and Environmental Sciences*, **3**(1), 68-78.
- Periyasamy, A. P. (2024). Recent advances in the remediation of textile-dye-containing wastewater: Prioritizing human health and sustainable wastewater treatment. Sustainability, 16(2), 495.

- Pindiga, N. Y., Abubakar, A., Danbature, W. L. and Yakubu, U. (2023). Green synthesis and characterization of iron nanoparticles from the leaf extract of *Khaya senegalensis* (Mahogany) and its antimicrobial activity. *Letters in Applied NanoBioScience*, **12**(3), 86
- Prakash, S., Elavarasan, N., Venkatesan, A., Subashini, K., Sowndharya, M. and Sujatha, V. (2018). Green synthesis of copper oxide nanoparticles and its effective applications in Biginelli reaction, BTB photodegradation and antibacterial activity. *Advanced Powder Technology*, **29**(12), 3315-3326.
- Prasad, C., Yuvaraja, G. and Venkateswarlu, P. (2017). Biogenic synthesis of Fe₃O₄ magnetic nanoparticles using *Pisum sativum* peels extract and its effect on magnetic and Methyl orange dye degradation studies. *Journal of Magnetism and Magnetic Materials*, **424**, 376-381.
- Roy, A., Singh, V., Sharma, S., Ali, D., Azad, A. K., Kumar, G. and Emran, T. B. (2022). Antibacterial and dye degradation activity of green synthesized iron nanoparticles. *Journal of Nanomaterials*, **2022**(1), 1-6.
- Sayed, K., Mohtar, W. W., Hanafiah, Z. M., Bithia, A. S., & Imad, W. A. A. Q. (2024). Removal of pharmaceuticals from municipal wastewater using Malaysian Ganoderma Lucidum Fungal Strain. *J Kejuruter*, **36**, 1467-1476.
- Sayed, K., Mohtar, W. H. M. W., Hanafiah, Z. M., Wan, W. A. A. Q. I., Abd Manan, T. S. B., & Sharif, S. A. B. M. (2024). Simultaneous enhanced removal of pharmaceuticals and hormone from wastewaters using series combinations of ultra-violet irradiation, bioremediation, and adsorption technologies. *Journal of Water Process Engineering*, **57**, 104589.
- Selvanarayanan, R., Rajendran, S., Pappa, C. K., & Thomas, B. (2024). Wastewater recycling to enhance environmental quality using fuzzy embedded with RNN-IOT for sustainable coffee farming. *Global Nest Journal*, **26**(8).
- Shahadat, A., Ahmed, W., Haroon, U. and Ahmed, K. (2024). Utilization of *Azadirachta Indica* Latex for Synthesis of Silver Nanoparticles its Application in Photocatalytic Degradation of Methylene Blue Dye. *Journal of Sustainable Environment*, **2**(3), 20-27.
- Sirdeshpande, K. D., Sridhar, A., Cholkar, K. M. and Selvaraj, R. (2018). Structural characterization of mesoporous magnetite nanoparticles synthesized using the leaf extract of *Calliandra haematocephala* and their photocatalytic degradation of malachite green dye. *Applied Nanoscience*, **8**, 675-683.
- Solomon, R. V., Lydia, I. S., Merlin, J. P. and Venuvanalingam, P. (2012). Enhanced photocatalytic degradation of azo dyes using nano Fe₃O₄. *Journal of the Iranian Chemical Society*, **9**, 101-109.
- Stan, M., Lung, I., Soran, M. L., Leostean, C., Popa, A., Stefan, M. and Porav, A. S. (2017). Removal of antibiotics from aqueous solutions by green synthesized magnetite nanoparticles with selected agro-waste extracts. *Process Safety and Environmental Protection*, **107**, 357-372.
- Sudhakar, C., Poonkothai, M., Selvankumar, T., & Selvam, K. (2022). Facile synthesis of iron oxide nanoparticles using *Cassia auriculata* flower extract and accessing their photocatalytic degradation and larvicidal effect. Journal of Materials Science: Materials in Electronics, **33**(14), 11434-11445.

- Teoh, Y. P., Ooi, Z. X., Leong, S. S., Ng, P. T. and Liu, W. W. (2021). Green synthesis of iron oxide nanoparticle using coffee seed extract and its antibacterial activity. *Journal of Engineering Science*, 17(2), 19-29.
- Ting, A. S. Y. and Chin, J. E. (2020). Biogenic synthesis of iron nanoparticles from apple peel extracts for decolorization of malachite green dye. *Water, Air, & Soil Pollution*, **231**(6), 278.
- Tyagi, P. K., Gupta, S., Tyagi, S., Kumar, M., Pandiselvam, R., Daştan, S. D. and Arya, A. (2021). Green synthesis of iron nanoparticles from spinach leaf and banana peel aqueous extracts and evaluation of antibacterial potential. *Journal of nanomaterials*, **2021**(1), 4871453.
- Uncu Kirtiş, E. B., Yiğit Koçak, D., Elderviş, U., Tuna, S., & Bayraç, C. (2025). Green synthesis of iron oxide nanoparticles from extracts of *Daucus carota* subsp. sativus whole vegetable, peel, pomace, and juice and their application as antibacterial agents and Fenton-like catalysts. *International Journal of Food Science and Technology*, **60**(1), vvae035.
- Usha, V., Amutha, E., Pushpalaksmi, E., Samraj, J. J., Rajaduraipandian, S., Gandhimathi, S. and Annadurai, G. (2022). Green synthesis and characterization of antibacterial studies by iron oxide nanoparticles using *Carica papaya* leaf extract. *Journal of Applied Sciences and Environmental Management*, **26**(3), 421-427.
- Velusamy, P., Das, J., Pachaiappan, R., Vaseeharan, B., & Pandian, K. (2015). Greener approach for synthesis of antibacterial silver nanoparticles using aqueous solution of neem gum (*Azadirachta indica L.*). *Industrial crops and products*, **66**, 103-109.
- VG, V. K., & Prem, A. A. (2018). Green synthesis and characterization of iron oxide nanoparticles using *Phyllanthus Niruri* extract. *Oriental Journal of Chemistry*, **34**(5).
- Vinay, C. H., Goudanavar, P., Acharya, A., Ahmed, M. G. and Kumar, P. S. (2018). Development and characterization of orange peel extract based nanoparticles. *Asian Journal of Pharmaceutical Research*, **8**(2), 71-77.
- Yazdani, F., & Seddigh, M. (2016). Magnetite nanoparticles synthesized by co-precipitation method: The effects of various iron anions on specifications. *Materials Chemistry and Physics*, **184**, 318-323.
- Zambri, N. D. S., Taib, N. I., Abdul Latif, F., & Mohamed, Z. (2019). Utilization of neem leaf extract on biosynthesis of iron oxide nanoparticles. *Molecules*, **24**(20), 3803.